

University of New Mexico

UNM Digital Repository

Branch Mathematics and Statistics Faculty and
Staff Publications

Branch Academic Departments

1999

PSEUDOSPECTRAL SOLUTION OF THE TWO-DIMENSIONAL NAVIER-STOKES EQUATIONS IN A DISK

Evangelos A. Coutsias

David J. Torres

Follow this and additional works at: https://digitalrepository.unm.edu/math_fsp



Part of the [Mathematics Commons](#)

Recommended Citation

SIAM Journal on Scientific Computing, 21(1): 378-403

This Article is brought to you for free and open access by the Branch Academic Departments at UNM Digital Repository. It has been accepted for inclusion in Branch Mathematics and Statistics Faculty and Staff Publications by an authorized administrator of UNM Digital Repository. For more information, please contact disc@unm.edu.

PSEUDOSPECTRAL SOLUTION OF THE TWO-DIMENSIONAL NAVIER–STOKES EQUATIONS IN A DISK*

D. J. TORRES[†] AND E. A. COUTSIAS[‡]

Abstract. An efficient and accurate algorithm for solving the two-dimensional (2D) incompressible Navier–Stokes equations on a disk with no-slip boundary conditions is described. The vorticity-stream function formulation of these equations is used, and spatially the vorticity and stream functions are expressed as Fourier–Chebyshev expansions. The Poisson and Helmholtz equations which arise from the implicit-explicit time marching scheme are solved as banded systems using a postconditioned spectral τ -method. The polar coordinate singularity is handled by expanding fields radially over the entire diameter using a parity modified Chebyshev series and building partial regularity into the vorticity. The no-slip boundary condition is enforced by transferring one of the two boundary conditions imposed on the stream function onto the vorticity via a solvability constraint. Significant gains in run times were realized by parallelizing the code in message passage interface (MPI).

Key words. spectral methods, coordinate singularity, parallel

AMS subject classifications. 76D05, 35Q30, 65M70, 65N35

PII. S1064827597330157

1. Introduction. An efficient and accurate algorithm for solving the 2D incompressible Navier–Stokes equations on a disk with no-slip boundary conditions is presented. The vorticity-stream function formulation of these equations is employed.

Spatially, the vorticity and stream functions are expressed as Fourier–Chebyshev expansions. The temporal evolution treats the nonlinear terms explicitly and the diffusion terms implicitly. The third-order stiffly stable scheme used for marching the solution forward in time requires the solution of a Poisson and a Helmholtz equation each time step. Since Fourier modes decouple, solving each of these elliptical equations amounts to solving a singular ordinary differential equation (ODE) for each Fourier mode, which is accomplished using the Chebyshev τ -method (Boyd [3]). The matrices that arise from these are transformed to banded form using a variation on the method developed by Coutsias et al. [7]. As such, only $\mathcal{O}(NM \log(NM))$ operations are required to advance the solution one time step, where N is the number of Fourier modes and M is the number of Chebyshev modes, accounting for the fast Fourier transform–fast cosine transform (FFT-FCT) (Temperton [20]) required to evaluate the nonlinear terms (Canuto et al. [4]).

Poisson’s equation can be solved accurately in spite of the polar coordinate singularity. However, the singularity does degrade the accuracy of the Helmholtz equation for high Reynolds numbers. The singularity has been investigated by several authors in a spectral τ , Galerkin, and collocation context; namely, Gottlieb and Orszag [11], Eisen et al. [9], Fornberg [10], Huang and Sloan [12], Orszag [16], Shen

*Received by the editors November 14, 1997; accepted for publication (in revised form) November 9, 1998; published electronically September 22, 1999. This work was partially supported by DOE grant DE-FG03-92ER25128 and by NOAA Climate and Global Change program grant NA56GP0219. This work was performed in part at the Mathematics Department and Albuquerque High Performance Computing Center, University of New Mexico, Albuquerque, and at the Physics Department and Geophysical Research Center, New Mexico Institute of Mining and Technology, Socorro, NM 87801. <http://www.siam.org/journals/sisc/21-1/33015.html>

[†]Theoretical Division, Los Alamos National Laboratory, Los Alamos, NM 87545 (dortres@lanl.gov).

[‡]Dept. of Mathematics and Statistics, University of New Mexico, Albuquerque, NM 87131 (vageli@math.unm.edu).

[19], Matsushima and Marcus [13], and Verkley [22, 23]. Several algorithms for three-dimensional (3D) cylindrical geometries are discussed in Priymak [17].

Gottlieb and Orszag [11] propose using an even Chebyshev expansion for even Fourier modes and an odd Chebyshev expansion for odd Fourier modes,

$$u_n = \sum_{\substack{k=0 \\ n+k \text{ even}}}^M a_{nk} T_k(r), \quad 0 \leq r \leq 1,$$

in computing eigenvalues of Bessel's equation,

$$(1) \quad u_n'' + \frac{1}{r} u_n' - \frac{n^2}{r^2} u_n = -\lambda u_n,$$

since the eigenfunctions of (1) inherit the parity of the Fourier mode, n . In addition, they find that convergence improves if a boundary condition is imposed at the center, $u_n'(0) = 0$ for $n \neq 1$.

Eisen et al. [9] also propose using even and odd expansions in solving the cylindrical Poisson, $-\nabla^2 u = f$, and Helmholtz equation

$$(2) \quad -\nabla^2 u + \lambda u = f$$

with a spectral collocation method. However, they expand over the interval $-1 \leq r \leq 1$. The expansion is constructed by extending a function $f_n(r)$, originally defined on $[0, 1]$ to $[-1, 1]$, using

$$(3) \quad f_n(-r) = \begin{cases} f_n(r) & \text{if } n \text{ even,} \\ -f_n(r) & \text{if } n \text{ odd,} \end{cases}$$

where n is the Fourier mode. The pole condition $u_n(0) = 0$ is suggested for Fourier modes $n \neq 0$. For $n = 0$, the pole conditions

$$-2 \frac{d^2 u_0}{dr^2} \Big|_{r=0} = f_0(0) \quad \text{and} \quad -2 \frac{d^2 u_0}{dr^2} \Big|_{r=0} + \lambda u_0|_{r=0} = f_0(0)$$

are used for the Poisson and Helmholtz equations, respectively.

Eisen et al. [9] also investigate the handling of the polar coordinate singularity by mapping the unit disk onto a rectangle with a monomial expansion

$$u(r, \theta) = \sum_{n=0}^M \sum_{k=-M+1}^M a_{nk} \Phi_{nk}^\circ$$

in the spectral collocation context, where $\Phi_{nk}^\circ = r^n e^{ik\theta}$. While spectral accuracy is achieved for $N \leq 16$, rounding errors contaminate the results for large values of N .

A collocation approach is described by Huang and Sloan [12] for computing eigenvalues of Bessel's equation (1) using a Chebyshev expansion on $0 \leq r \leq 1$. Spectral convergence for the first and second eigenvalue for different Fourier modes is realized when

$$(4) \quad u_n(0) = 0, n \neq 0, \quad u_0'(0) = 0$$

are enforced. A spectrally accurate solution of the Helmholtz equation (2) is also achieved with an equivalent form of the pole condition (4).

Building additional regularity into the solution

$$f(r, \theta) = \sum f_n(r) r^n e^{in\theta}$$

is studied by Orszag et al. [16] and in a spherical context by Merilees [14]. Such regularity is justified since the n th Fourier coefficient of a function $f(r, \theta)$ decays as r^n near the origin. However, generating the expansion coefficients $f_n(r)$ from $f(r, \theta)$ is an ill-conditioned operation as $r \rightarrow 0$ for large truncations on $0 \leq r \leq 1$.

Shen [19] uses an efficient spectral-Galerkin approach in solving the Helmholtz equation on a unit disk. He enforces the boundary condition $u_n(0) = 0, n \neq 0$ for Fourier modes n greater than zero by using basis functions

$$\phi_i(x) = L_i(x) - L_{i+1}(x), \quad i = 0, 1, \dots, N - 2,$$

where L_i represents either the i th degree Legendre or the Chebyshev polynomial. A regularity boundary condition for $n = 0$ is not enforced. The Galerkin method insures that the regularity condition $u_n(0) = 0, n \neq 0$ will automatically be satisfied.

Matsushima and Marcus [13] treat the singularity in an elegant way using the basis $Q_n^m(\alpha, \beta; r) e^{im\theta}$ (with $m + n$ even), where $Q_n^m(\alpha, \beta; r)$ is an orthogonal polynomial which behaves as $\mathcal{O}(r^{|m|})$ as $r \rightarrow 0$. Verkley [22, 23] works along similar lines by using the basis functions $r^{|m|} P^{(0, |m|)}(2r^2 - 1) e^{im\theta}$, where $P^{(0, |m|)}$ are the Jacobi polynomials. Although such expansions share with the Chebyshev method efficient representations of the relevant differential operators, as they all rely on orthogonal polynomials of a hypergeometric type (see [7]), an efficient implementation for large truncations requires a fast transform on these bases which is not readily available.

The treatment of the Helmholtz polar coordinate singularity here follows Eisen et al. [9] (see also Fornberg [10]) in expanding solutions over the interval $-R \leq r \leq R$ rather than $0 \leq r \leq R$. From a Navier–Stokes perspective, the expansion also puts less of a constraint on one’s time step, due to the distribution of the Gaussian quadrature nodes. However, the implemented solution of the Helmholtz equation proposed here builds *partial* regularity into the vorticity, similar to the coordinate transformation used in [18] for velocity and pressure. If ω_n represents the n th Fourier mode of vorticity, we assume $\omega_n = r^2 s_n$ for $n \geq 2$ and $\omega_1 = r s_1$, and solve for s_n rather than ω_n in the Helmholtz equation. While ideally $\omega_n = r^n s_n$, we are precluded from making such an assignment due to severe ill-conditioning which arises in the FFT. Finding an optimal α , where $\omega_n = r^\alpha s_n$, is a matter of balancing the conditioning between the FFT and the Helmholtz equation. Our choice of partial regularity represents an adequate compromise while allowing a lean implementation. An optimal analysis will be pursued later.

In addition, no-slip boundary conditions are constructed and imposed differently than methods used by other authors: Dennis and Quartapelle [8] and Coutsias and Lynov [5] solve the incompressible fluid equations in a vorticity-stream function formulation.

The code is written in Fortran 90 and is parallelized using the MPI parallel language. Since Fourier modes can be handled independently of each other, the Poisson and Helmholtz equations can be solved independently on each processor for a particular range of Fourier modes. In addition, the potential memory capacity is enhanced in parallel, since each processor only holds a fraction of the total number of Fourier modes. No communication between processors is required, except when non-linear terms need be multiplied. Multiplication is performed by transforming fields

TABLE 1
Computational speed-up $m \times n$ denotes m Chebyshev modes and n Fourier modes.

Processors	256x256	512x512	1024x512	1000x800
1	1.00	1.00	1.00	1.00
2	1.35	1.42	1.41	1.51
4	2.43	2.78	2.74	3.06
6	3.54	4.01	3.98	4.51
8	4.33	5.00	5.02	5.75
10	5.39	6.05	6.00	6.83
12	6.21	6.79	6.90	8.16
14	6.71	7.92	7.70	9.35
16	7.00	8.67	8.49	10.11

to point space using a parallel FFT-FCT algorithm, multiplying the fields in point space in transposed form, and transforming the product back into mode space. Using our implementation in MPI, we realize significant gains in computational speed by parallelizing the code, especially at larger truncations, as Table 1 shows. The code developed for one processor eliminates inefficiencies introduced by the parallelization and thus differs from the parallel code.

The paper is organized as follows: Section 2 discusses the incompressible Navier–Stokes equations and the implicit-explicit time discretization used to solve them. Aspects of the Fourier–Chebyshev spatial expansion are also described. Appendix A discusses an efficient technique for solving ODEs using the spectral τ -method. Section 3 applies the technique to the Poisson and Helmholtz operators which arise from the vorticity-stream function formulation and the implicit time discretization. We also discuss how imposing regularity on the vorticity improves the conditioning of the linear systems. Section 4 discusses the construction and imposition of boundary constraints on the vorticity. Section 5 summarizes the work and ends with a numerical calculation of a vortex dipole colliding with a cylindrical wall.

2. Incompressible Navier–Stokes equations. This section discusses the solution of the 2D incompressible Navier–Stokes equations in the vorticity-stream function formulation, using a Fourier–Chebyshev spectral expansion. The equations are solved in a disk geometry, $0 \leq r \leq R$, $0 \leq \theta < 2\pi$.

Let \vec{u} , ρ , p , and ν denote the velocity field, density, pressure, and kinematic viscosity, respectively. The incompressible Navier–Stokes equations include the momentum equation

$$(5) \quad \frac{\partial \vec{u}}{\partial t} + \vec{u} \cdot \nabla \vec{u} = -\frac{1}{\rho} \nabla p + \nu \nabla^2 \vec{u}$$

and the conservation of mass equation

$$(6) \quad \nabla \cdot \vec{u} = 0.$$

Taking the curl of (5) yields

$$(7) \quad \frac{\partial \omega}{\partial t} + J(\omega, \psi) = \nu \nabla^2 \omega,$$

where ω is the vorticity in the z -direction and ψ , the stream function, is defined by

$$(8) \quad \vec{u} = \nabla \psi \times \hat{e}_z.$$

The Jacobian $J(\omega, \psi)$ is defined by

$$(9) \quad J(\omega, \psi) = \frac{1}{r} \left[\frac{\partial \omega}{\partial r} \frac{\partial \psi}{\partial \theta} - \frac{\partial \omega}{\partial \theta} \frac{\partial \psi}{\partial r} \right]$$

and is computed at the origin using Cartesian coordinates,

$$J(\omega, \psi) = \frac{\partial \omega}{\partial x} \frac{\partial \psi}{\partial y} - \frac{\partial \psi}{\partial x} \frac{\partial \omega}{\partial y}.$$

To find the x - and y -derivative at the origin of a function defined in terms of r and θ , it is easiest to set θ equal to 0 and $\frac{\pi}{2}$, respectively, and find the r -derivative.

By taking the curl of (8), one obtains

$$(10) \quad \nabla^2 \psi = -\omega.$$

Equations (7) and (10) form the vorticity-stream function formulation of the incompressible Navier–Stokes equations (5) and (6).

2.1. Time integration scheme. The presence of both nonlinear and linear terms in (7) suggests the use of an implicit-explicit time integration scheme. The diffusive term is treated implicitly for stability reasons, while the nonlinear term is treated explicitly for simplicity. Following Ascher et al. [2], we employ a third order semi-implicit backward differentiation formula time integration scheme (a stiffly stable scheme). At each time step, the following equations are solved (the superscript denotes the time level):

$$(11) \quad \nabla^2 \psi^k = -\omega^k,$$

$$(12) \quad (1 - \nu \delta t \nabla^2) \omega^{k+1} = \frac{6}{11} \left\{ 3\omega^k - \frac{3}{2}\omega^{k-1} + \frac{1}{3}\omega^{k-2} + \delta t(3F^k - 3F^{k-1} + F^{k-2}) \right\},$$

where $F^k = -J(\omega^k, \psi^k)$ and δt is the time step. Thus one Poisson and one Helmholtz equation are solved at each time step.

2.2. Fourier–Chebyshev expansion. The spatial (r, θ) dependence of ω and ψ is treated spectrally. Due to the periodicity in the θ direction, ψ and ω are expanded in a Fourier series,

$$(13) \quad \psi(r, \theta) = \sum_{n=0}^{\frac{N}{2}} \psi_n^c(r) \cos n\theta + \sum_{n=1}^{\frac{N}{2}-1} \psi_n^s(r) \sin n\theta,$$

$$(14) \quad \omega(r, \theta) = \sum_{n=0}^{\frac{N}{2}} \omega_n^c(r) \cos n\theta + \sum_{n=1}^{\frac{N}{2}-1} \omega_n^s(r) \sin n\theta.$$

The term ψ_n will be used to denote either ψ_n^c or ψ_n^s and similarly for ω_n .

A choice for the orthogonal polynomial basis must be made for the radial expansion. The Chebyshev polynomials prove useful in this regard. The Chebyshev expansion coefficients for a function of one variable can be generated efficiently in $\mathcal{O}(M \log(M))$ operations using a fast cosine transform, M being the number of expansion coefficients. The functions ψ_n and ω_n are expanded in a Chebyshev series

defined on the entire interval $-R \leq r \leq R$, as opposed to the half-interval $0 \leq r \leq R$. For Gauss–Lobatto quadrature points, the grid is $r_i = R \cos(\frac{\pi i}{M})$, $0 \leq i \leq M$. Note that only the half-interval $[0, R]$ is used in computing with fields in point space. This grid is resolved near $r = R$, where the grid spacing is $\mathcal{O}(\frac{1}{M^2})$, and sparse near $r = 0$, where the grid spacing is $\mathcal{O}(\frac{1}{M})$. The grid spacing near the origin does not overconstrain the time step by the Courant–Friedrichs–Lewy condition. Also, it is observed that the condition numbers for the spectral matrices that arise improve if ψ_n and ω_n are expanded over the entire interval $[-R, R]$, compared to the half interval $[0, R]$. We radially expand ψ_n and ω_n on $[-R, R]$, following Eisen et al. [9] and using equation (3) to arrive at the following expressions:

$$(15) \quad \psi_n(r) = \psi_n(Rx) = \sum_{\substack{m=0 \\ n+m=\text{even}}}^{m=M} \psi_{nm} T_m(x), \quad \omega_n(r) = \sum_{\substack{m=0 \\ n+m=\text{even}}}^{m=M} \omega_{nm} T_m(x).$$

Here $T_m(x)$ represents the Chebyshev polynomial of order m , $-1 \leq x \leq 1$.

2.3. Poisson and Helmholtz equations. Advancing the Navier–Stokes equations in time requires the solution of a Poisson (11) and a Helmholtz (12) equation. In cylindrical coordinates, Poisson’s equation $\nabla^2 \psi = -\omega$ assumes the form

$$\left[\frac{1}{r} \frac{\partial}{\partial r} \left(r \frac{\partial \psi}{\partial r} \right) + \frac{1}{r^2} \frac{\partial^2 \psi}{\partial \theta^2} \right] = -\omega(r, \theta),$$

$$0 \leq r \leq R, \quad 0 \leq \theta < 2\pi.$$

Multiplying by r^2 , substituting the Fourier expansions for ψ and ω , and using the orthogonality of the sine and cosine functions, one arrives at the following ODEs,

$$(16) \quad r^2 \frac{d^2 \psi_n}{dr^2} + r \frac{d\psi_n}{dr} - n^2 \psi_n = -r^2 \omega_n, \quad 0 \leq n \leq \frac{N}{2}.$$

In cylindrical coordinates, the Helmholtz equation assumes the form

$$(17) \quad \omega(r, \theta) - \epsilon \left[\frac{\partial^2 \omega}{\partial r^2} + \frac{1}{r} \frac{\partial \omega}{\partial r} + \frac{1}{r^2} \frac{\partial^2 \omega}{\partial \theta^2} \right] = f(r, \theta),$$

where $\epsilon \equiv \nu \delta t$ and $f(r, \theta)$ denotes the right hand side of (12). Again, as with Poisson’s equation, one generates a set of ODEs similar to those of Poisson’s equation,

$$(18) \quad r^2 \omega_n - \epsilon \left[r^2 \frac{d^2 \omega_n}{dr^2} + r \frac{d\omega_n}{dr} - n^2 \omega_n \right] = r^2 f_n, \quad 0 \leq n \leq \frac{N}{2}.$$

2.4. Boundary conditions. No-slip boundary conditions are imposed. A velocity field \vec{u} is composed of a radial and tangential component,

$$\vec{u} = (u \hat{e}_r + v \hat{e}_\theta) = \left(\frac{1}{r} \frac{\partial \psi}{\partial \theta} \hat{e}_r - \frac{\partial \psi}{\partial r} \hat{e}_\theta \right).$$

The no-slip constraint is $v|_{r=R} = U$, which translates (in terms of the stream function) into

$$(19) \quad \left. \frac{\partial \psi}{\partial r} \right|_{r=R} = -U.$$

In addition, the normal component of the velocity should be zero at the boundary ($u|_{r=R} = 0$), which translates into

$$(20) \quad \left. \frac{\partial \psi}{\partial \theta} \right|_{r=R} = 0.$$

In terms of the individual Fourier components, the no-slip constraints (19) are

$$(21) \quad \left. \frac{d\psi_n}{dr} \right|_{r=R} = 0 \quad n > 0, \quad \left. \frac{d\psi_0}{dr} \right|_{r=R} = -U$$

and the normal constraints (20) are

$$(22) \quad \psi_n|_{r=R} = 0 \quad n > 0.$$

Two sets of boundary conditions on ψ_n , $n > 0$, (21)–(22), cause the Poisson equation to be overdetermined. This difficulty is resolved in section 4.

2.5. Evolution diagnostics. The temporal evolution of the energy (E), enstrophy (Ω), circulation (C), and angular momentum (L) in a disk with no-slip boundary conditions can be derived from (5)–(7):

$$(23) \quad \frac{dE}{dt} = \nu C \omega_0|_{r=R} - \nu \Omega,$$

$$(24) \quad \frac{d\Omega}{dt} = 2\pi R \nu \left. \frac{\partial(\omega^2)_0}{\partial r} \right|_{r=R} - 2\nu \int_0^{2\pi} \int_0^R \left[\left(\frac{\partial \omega}{\partial r} \right)^2 + \left(\frac{1}{r} \frac{\partial \omega}{\partial \theta} \right)^2 \right] r dr d\theta,$$

$$(25) \quad \frac{dC}{dt} = 2\pi \nu \left. \frac{d\omega_0}{dr} \right|_{r=R},$$

$$(26) \quad \frac{dL}{dt} = 2\pi R^2 \nu \omega_0|_{r=R} - 2\nu C,$$

where

$$E = \frac{1}{2} \int \int_{r \leq R} \vec{u} \cdot \vec{u} dS, \quad \Omega = \int \int_{r \leq R} \omega^2 dS$$

and

$$C = \oint_{r=R} \vec{u} \cdot \vec{dl}, \quad L = \hat{e}_z \cdot \int \int_{r \leq R} r \hat{e}_r \times \vec{u} dS.$$

Following Coutsias and Lynov [5], these equations are used to track the temporal accuracy of the code.

3. Banding Poisson and Helmholtz operators. We will now apply the techniques of Appendix A to solve the Poisson (16) and Helmholtz ODEs (18). Applying the spectral τ -method to the Poisson equations in the standard way, one forms the system of equations (59)

$$(27) \quad \frac{1}{R^2} [-\mathbf{x}^2 \mathbf{D}^2 - \mathbf{x} \mathbf{D} + n^2 \mathbf{I}] \vec{\psi}_n = \mathbf{x}^2 \vec{\omega}_n,$$

where the convolution and differentiation matrices, \mathbf{x} and \mathbf{D} , transform the vector of coefficients for $f(x)$ into the vector of coefficients for $xf(x)$ and $\frac{df}{dx}$, respectively. Here (16) has been transformed to use the independent variable, $x = \frac{r}{R}$, $-1 \leq x \leq 1$. Letting

$$(28) \quad \vec{\psi}_n = \mathbf{P}^2 \vec{\psi}_n^*,$$

where \mathbf{P} is the postconditioner introduced in Appendix A, one obtains the banded system

$$(29) \quad \frac{1}{R^2} [-\mathbf{x}^2 \mathbf{D}^2 \mathbf{P}^2 - \mathbf{x} \mathbf{D} \mathbf{P}^2 + n^2 \mathbf{P}^2] \vec{\psi}_n^* = \mathbf{x}^2 \vec{\omega}_n.$$

For the Chebyshev polynomials,

$$\mathbf{P}^2 = \begin{bmatrix} 1 & 0 & 0 & 0 & \cdots & 0 \\ 0 & 1 & 0 & -\frac{1}{2} & \cdots & 0 \\ 0 & 0 & \frac{1}{2i} & 0 & -\frac{1}{2i} & 0 \\ \vdots & \vdots & 0 & \ddots & 0 & \frac{-1}{2M-4} \\ 0 & 0 & 0 & 0 & \frac{1}{2M-2} & 0 \\ 0 & 0 & 0 & 0 & 0 & \frac{1}{2M} \end{bmatrix} \begin{bmatrix} 1 & 0 & 0 & 0 & 0 & \cdots & 0 \\ 0 & 1 & 0 & 0 & 0 & \cdots & 0 \\ 0 & 0 & 1 & 0 & -\frac{1}{2} & \cdots & 0 \\ 0 & 0 & 0 & +\frac{1}{2i} & 0 & -\frac{1}{2i} & 0 \\ \vdots & \vdots & 0 & 0 & \ddots & 0 & \frac{-1}{2M-6} \\ 0 & 0 & 0 & 0 & 0 & \frac{1}{2M-4} & 0 \\ 0 & 0 & 0 & 0 & 0 & 0 & \frac{1}{2M-2} \end{bmatrix},$$

$$\mathbf{D} \mathbf{P}^2 = \begin{bmatrix} 0 & 1 & 0 & 0 & 0 & 0 & \cdots & 0 \\ 0 & 0 & 1 & 0 & -\frac{1}{2} & 0 & \cdots & 0 \\ 0 & 0 & 0 & +\frac{1}{4} & 0 & -\frac{1}{4} & 0 & 0 \\ 0 & 0 & 0 & 0 & +\frac{1}{2i} & 0 & -\frac{1}{2i} & 0 \\ 0 & 0 & 0 & 0 & 0 & \ddots & 0 & \frac{-1}{2M-6} \\ \vdots & \vdots & 0 & 0 & 0 & 0 & \frac{1}{2M-4} & 0 \\ 0 & 0 & 0 & 0 & 0 & 0 & 0 & \frac{1}{2M-2} \\ 0 & 0 & 0 & 0 & 0 & 0 & 0 & 0 \end{bmatrix},$$

$$\mathbf{D}^2 \mathbf{P}^2 = \begin{bmatrix} 0 & 0 & 1 & 0 & 0 & 0 \\ 0 & \vdots & 0 & 1 & 0 & 0 \\ 0 & 0 & 0 & 0 & \ddots & 0 \\ 0 & 0 & 0 & 0 & 0 & 1 \\ 0 & 0 & 0 & 0 & 0 & 0 \\ 0 & \cdots & 0 & 0 & 0 & 0 \end{bmatrix}, \quad \mathbf{x} = \begin{bmatrix} 0 & .5 & 0 & 0 & 0 & 0 \\ 1 & 0 & .5 & 0 & 0 & 0 \\ 0 & .5 & 0 & .5 & 0 & 0 \\ 0 & 0 & \ddots & 0 & \ddots & 0 \\ 0 & 0 & 0 & .5 & 0 & .5 \\ 0 & \cdots & 0 & 0 & .5 & 0 \end{bmatrix}.$$

We found that our postconditioned method required no special treatment for Poisson’s equation. Spectrally accurate solutions for this singular problem were obtained at large truncations M by solving the system (29) with boundary conditions.

However, the spectral accuracy of the postconditioned method solution was degraded for the Helmholtz equation

$$u - \epsilon \nabla^2 u = f$$

TABLE 2

Errors in a postconditioned solution of Helmholtz equation (17) with Dirichlet boundary conditions without regularity where $f(r, \theta)$ was generated by letting ω be the exact solution, $\epsilon = 1 \times 10^{-9}$, Fourier modes = 256, and a varying number of Chebyshev modes $-1 \leq x \leq 1$, $R = 1$.

$\omega(x, y)$	32	64	128	256	512	1024	2048
$\sin(x^2y)$	9(-15)	3(-14)	2(-13)	1(-12)	2(-12)	2(-11)	2(-11)
e^{-5r^2}	1(-11)	6(-15)	2(-13)	3(-14)	1(-12)	8(-12)	2(-12)
$\cos(\cos(x+y))$	6(-14)	2(-13)	2(-13)	3(-12)	9(-12)	5(-11)	1(-10)
$r^7 \sin(7\theta)$	3(-14)	8(-14)	1(-12)	3(-12)	2(-11)	8(-11)	2(-10)
e^{x+y+y^2}	2(-13)	8(-13)	2(-12)	2(-11)	6(-11)	3(-10)	2(-9)
$\sin(\pi r^2)$	9(-14)	3(-13)	5(-13)	5(-12)	1(-11)	5(-11)	1(-10)
$\cos(5r)$	4(-14)	2(-13)	1(-12)	2(-13)	1(-11)	3(-11)	2(-10)
$J_0(r)$	5(-14)	1(-13)	9(-14)	1(-12)	7(-12)	9(-11)	5(-11)

TABLE 3

Errors in postconditioned solution of Helmholtz equation (17) with Dirichlet boundary conditions with regularity where $f(r, \theta)$ was generated by letting ω be the exact solution: $\epsilon = 1 \times 10^{-9}$, Fourier modes = 256, and a varying number of Chebyshev modes $-1 \leq x \leq 1$, $R = 1$.

$\omega(x, y)$	32	64	128	256	512	1024	2048
$\sin(x^2y)$	2(-15)	1(-15)	5(-15)	7(-15)	1(-14)	1(-14)	2(-14)
e^{-5r^2}	9(-13)	2(-13)	9(-15)	1(-14)	2(-14)	3(-14)	8(-14)
$\cos(\cos(x+y))$	2(-12)	7(-13)	9(-14)	2(-14)	6(-15)	4(-14)	5(-14)
$r^7 \sin(7\theta)$	6(-15)	6(-15)	8(-15)	4(-14)	5(-14)	2(-13)	1(-13)
e^{x+y+y^2}	1(-11)	2(-12)	5(-14)	1(-13)	1(-13)	5(-13)	5(-13)
$\sin(\pi r^2)$	4(-12)	4(-13)	7(-14)	9(-15)	1(-14)	5(-14)	4(-14)
$\cos(5r)$	2(-12)	3(-14)	3(-14)	1(-14)	2(-14)	1(-13)	4(-14)
$J_0(r)$	8(-12)	2(-14)	3(-15)	1(-14)	8(-15)	1(-14)	2(-14)

on either $-1 \leq x \leq 1$ or $0 \leq x \leq 1$ for small $\epsilon \ll 1$, and large truncations. See Table 2 for the expansion interval $-1 \leq x \leq 1$. The degradation of accuracy is even more dramatic for $0 \leq x \leq 1$.

As epsilon becomes small, the Helmholtz ODEs (18) start to resemble

$$r^2 \omega_n = r^2 f_n(r).$$

Not surprisingly, the spectral operator r^2 , supplemented with tau constraints, becomes ill-conditioned as the truncation M increases. One would similarly find numerical inaccuracies if $r^2 f_n(r)$ was divided by r^2 in point space as $r \rightarrow 0$.

However, one can improve the situation by building regularity into the solution $\omega_n(r)$. See Table 3. Consider the equations (18). Different strategies are employed for different Fourier modes, n .

3.1. Fourier mode = 1. If $n = 1$, set $\omega_1(r) = rs_1(r)$. This is valid since $\omega_1(r)$ should decay like r near the origin. The equation now assumes the form

$$r^2(rs_1) - \epsilon \left[r^2 \frac{d^2(rs_1)}{dr^2} + r \frac{d(rs_1)}{dr} - rs_1 \right] = r^2 f_1,$$

or, after cancellation of r^2 ,

$$(30) \quad rs_1 - \epsilon \left[r \frac{d^2 s_1}{dr^2} + 3 \frac{ds_1}{dr} \right] = f_1.$$

Truncating the spectral expansions, one obtains the linear system

$$(31) \quad R\mathbf{x}\vec{s}_1 - \frac{\epsilon}{R} [\mathbf{x}\mathbf{D}^2 + 3\mathbf{D}] \vec{s}_1 = \vec{f}_1,$$

where $x = \frac{r}{R}$, $-1 \leq x \leq 1$. Finally, letting $\vec{s}_1 = \mathbf{P}^2 \vec{s}_1^*$ yields the system of equations

$$(32) \quad R\mathbf{x}\mathbf{P}^2 \vec{s}_1^* - \frac{\epsilon}{R} [\mathbf{x}\mathbf{D}^2 \mathbf{P}^2 + 3\mathbf{D}\mathbf{P}^2] \vec{s}_1^* = \vec{f}_1,$$

which is supplemented with a tau constraint arising from a boundary condition at $x = 1$. After solving for \vec{s}_1^* , $\vec{\omega}_1$ is recovered through

$$(33) \quad \vec{\omega}_1 = R\mathbf{x}\mathbf{P}^2 \vec{s}_1^*.$$

If ϵ is small, spurious modes present in \vec{s}_1^* , due to the near inversion of $\mathbf{x}\mathbf{P}^2$, are almost eliminated upon multiplication by $\mathbf{x}\mathbf{P}^2$.

3.2. Fourier mode ≥ 2 . If $n \geq 2$, set $\omega_n(r) = r^2 s_n(r)$. This is valid since $\omega_n(r)$ should decay as r^n near the origin. Upon substituting this form of $\omega_n(r)$ into (18) and cancelling r^2 , one obtains

$$(34) \quad r^2 s_n - \epsilon \left[r^2 \frac{d^2 s_n}{dr^2} + 5r \frac{ds_n}{dr} + (4 - n^2)s_n \right] = f_n.$$

Letting $\vec{s}_n = \mathbf{P}^2 \vec{s}_n^*$ yields the linear system

$$(35) \quad R^2 \mathbf{x}^2 \mathbf{P}^2 \vec{s}_n^* - \epsilon [\mathbf{x}^2 \mathbf{D}^2 \mathbf{P}^2 + 5\mathbf{x}\mathbf{D}\mathbf{P}^2 + (4 - n^2)\mathbf{P}^2] \vec{s}_n^* = \vec{f}_n.$$

The expansion $\vec{\omega}_n$ is recovered via

$$(36) \quad \vec{\omega}_n = R^2 \mathbf{x}^2 \mathbf{P}^2 \vec{s}_n^*.$$

If ϵ is small, spurious modes present in \vec{s}_n^* , due to the near inversion of $\mathbf{x}^2 \mathbf{P}^2$, are almost eliminated upon multiplication by $\mathbf{x}^2 \mathbf{P}^2$.

3.3. Fourier mode = 0. Fourier mode $n = 0$ requires more care. While no immediate regularity can be built into $\omega_0(r)$, regularity can be built into the derivative of $\omega_0(r)$. Start by dividing (18) by r^2 ,

$$(37) \quad \omega_0 - \epsilon \left[\frac{d^2 \omega_0}{dr^2} + \frac{1}{r} \frac{d\omega_0}{dr} \right] = f_0.$$

Differentiating and multiplying by r^2 , one forms an ODE in $\frac{d\omega_0}{dr}$,

$$r^2 \frac{d\omega_0}{dr} - \epsilon \left[r^2 \frac{d^3\omega_0}{dr^3} + r \frac{d^2\omega_0}{dr^2} - \frac{d\omega_0}{dr} \right] = r^2 \frac{df_0}{dr}.$$

Now set

$$(38) \quad \frac{d\omega_0}{dr} = r s_0.$$

This assignment is valid since ω_0 will have an expansion of the form

$$\omega_0 = a_0 + a_2 r^2 + a_4 r^4 + \dots$$

Form (38) is dictated by the Neumann boundary conditions (63) on ω_0 . Substituting and simplifying, it follows that

$$(39) \quad r s_0 - \epsilon \left[r \frac{d^2 s_0}{dr^2} + 3 \frac{ds_0}{dr} \right] = \frac{df_0}{dr}.$$

This operator is the same operator used with Fourier mode, $n = 1$,

$$(40) \quad R \mathbf{xP}^2 \vec{s}_0^* - \frac{\epsilon}{R} [\mathbf{xD}^2 \mathbf{P}^2 + 3 \mathbf{DP}^2] \vec{s}_0^* = \frac{\mathbf{D} \vec{f}_0}{R},$$

where $\vec{s}_0 = \mathbf{P}^2 \vec{s}_0^*$. The term $\frac{d\vec{\omega}_0}{dx}$ is recovered via

$$(41) \quad \frac{d\vec{\omega}_0}{dx} = R^2 \mathbf{xP}^2 \vec{s}_0^*$$

and $\vec{\omega}_0$ is recovered via

$$(42) \quad \vec{\omega}_0 = \mathbf{B} \frac{d\vec{\omega}_0}{dx}$$

by (68). The first component of $\vec{\omega}_0$ can be determined using (37). Equation (37) can be written in the form

$$\omega_0 - \epsilon \left[r \frac{ds_0}{dr} + 2s_0 \right] = f_0$$

using (38). Now evaluate at $r = R$ or $x = 1$,

$$(43) \quad \omega_0|_{x=1} = f_0|_{x=1} + \epsilon \left[\frac{ds_0}{dx} + 2s_0 \right] \Big|_{x=1}.$$

3.4. Conditioning. In this section, we discuss the conditioning of the matrices arising from the Helmholtz ODE (18) matrices using the substitutions (33), (36), and (41). All linear systems (32), (35), and (40) involve the solution of a banded system

$$(44) \quad \mathbf{A} \vec{s}^* = \vec{f}$$

for \vec{s}^* , followed by multiplication by $\mathbf{x}^l \mathbf{P}^2$, $l = 1, 2$,

$$(45) \quad \vec{u} = \mathbf{x}^l \mathbf{P}^2 \vec{s}^*.$$

TABLE 4

Condition numbers using l_2 norm, $n = 3$ or $n = 10$, for $\epsilon = 1 \times 10^{-9}$ for varying Chebyshev truncations. $\mathbf{A} = \mathbf{x}^2\mathbf{P}^2 - \epsilon[\mathbf{x}^2\mathbf{D}^2\mathbf{P}^2 + 5\mathbf{x}\mathbf{D}\mathbf{P}^2 + (4 - n^2)\mathbf{P}^2]$ with Dirichlet boundary condition, $\tau_1 \cdot \mathbf{x}^2\mathbf{P}^2$ $\tilde{\mathbf{A}} = \mathbf{x}^2\mathbf{P}^2 - \epsilon[\mathbf{x}^2\mathbf{D}^2\mathbf{P}^2 + \mathbf{x}\mathbf{D}\mathbf{P}^2 - n^2\mathbf{P}^2]$ with Dirichlet boundary condition, $\tau_1 \cdot \mathbf{P}^2$.

Truncation	$\ \mathbf{A}\ $ $\ \mathbf{x}^2\mathbf{P}^2\mathbf{A}^{-1}\ $	$\ \tilde{\mathbf{A}}\ $ $\ \tilde{\mathbf{A}}^{-1}\ $
8	2.8, 2.4	1.8×10^3 , 3.0×10^3
16	3.9, 3.8	2.8×10^4 , 3.6×10^4
32	5.3, 5.3	4.3×10^5 , 4.8×10^5
64	7.3, 7.4	6.7×10^6 , 7.0×10^6
128	9.0, 10.3	9.8×10^7 , 1.0×10^8
256	5.8, 14.5	7.3×10^8 , 7.3×10^8
512	6.6, 20.2	3.1×10^9 , 7.4×10^9
1024	8.7, 27.8	5.0×10^{10} , 1.1×10^{11}

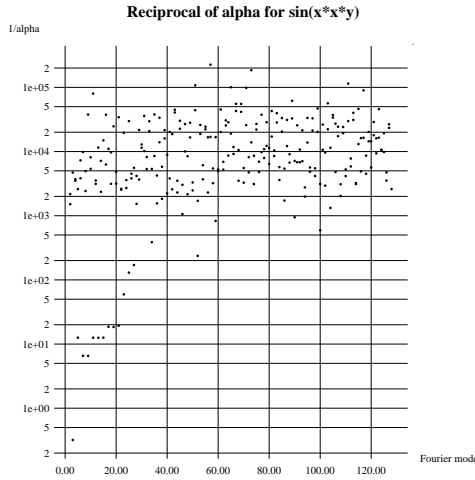


FIG. 1. Reciprocal of α , $\alpha = \frac{\|\mathbf{x}^2\mathbf{P}^2\vec{s}_n^*\|}{\|\vec{s}_n^*\|}$, $n \geq 2$, where s_n^* is generated by solving (35) with Dirichlet boundary conditions with right hand side corresponding to exact solution $\omega = \sin(x^2y)$, $-1 \leq r \leq 1$ using 1024 Chebyshev modes.

Neglecting higher order errors, the effective condition number is

$$\frac{\|\vec{\Delta}u\|}{\|\vec{u}\|} \leq \frac{1}{\alpha} \|\mathbf{x}^l\mathbf{P}^2\mathbf{A}^{-1}\| \|\mathbf{A}\| (\delta f + 2\delta A),$$

where δf and δA represent the relative errors in \vec{f} and \mathbf{A} . Appendix B supplies the details.

Table 4 shows the condition numbers of the relevant matrices for systems with and without regularity on $-1 \leq x \leq 1$, with Dirichlet boundary conditions for small ϵ . Values (for both the sine and cosine) of $\frac{1}{\alpha}$ are graphed versus the Fourier mode in Figures 1 and 2 for exact solutions, $\omega = \sin(x^2y)$ and $\omega = e^{x+y+y^2}$. Compare the product of column 2 of Table 4 with $\frac{1}{\alpha}$ from Figures 1 and 2 with column 3 of Table 4. Obviously we cannot generate α for all solutions, but for these exact solutions, one

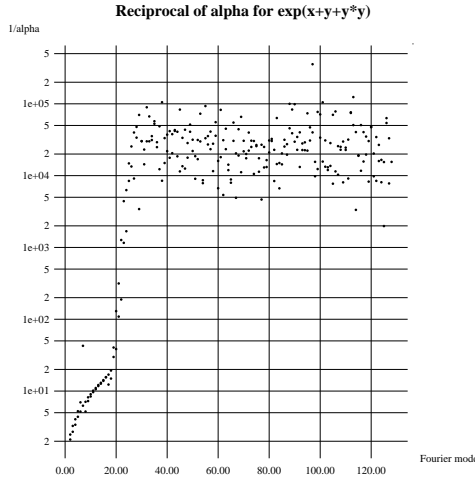


FIG. 2. Reciprocal of α , $\alpha = \frac{\|\mathbf{x}^2 \mathbf{P}^2 \mathbf{s}_n^*\|}{\|\mathbf{s}_n^*\|}$, $n \geq 2$, where \mathbf{s}_n^* is generated by solving (35) with Dirichlet boundary conditions with right hand side corresponding to exact solution $\omega = e^{x+y+y^2}$, $-1 \leq r \leq 1$ using 1024 Chebyshev modes.

has solved the Helmholtz equation with regularity, with condition numbers that are four orders of magnitude better for a Chebyshev truncation of 1024 for the majority of Fourier modes. Tables 2 and 3 show that we have improved the accuracy of other smooth solutions. The accuracy without regularity would suffer even more dramatically if an expansion interval of $0 \leq r \leq 1$ was used. The condition numbers in Table 4 do not seem to vary much between Fourier modes of the same parity since $\epsilon \ll 1$.

4. Boundary conditions. Two sets of boundary conditions on ψ ((21)–(22)) $n > 0$, cause the Poisson equation to be overdetermined.

In addition, no boundary conditions are imposed on the vorticity, ω . One can resolve this dilemma by transferring one set of boundary constraints on ψ onto ω . This scheme uses a matrix approach and differs from the no-slip boundary schemes used by Dennis and Quartapelle [8] and Coutsias and Lynov [5].

It is efficient in that only $\mathcal{O}(M)$ operations are required to compute the boundary constraint on $\vec{\omega}_n$ for each Fourier mode. Since the boundary constraints on $\vec{\omega}_n$ will not be Dirichlet constraints, the condition numbers shown in Table 4 will change. However, benefits of the partial regularity built into $\vec{\omega}_n$ should continue to improve the accuracy of solutions.

Let $\vec{\tau}_1$ denote the row vector which evaluates a vector of expansion coefficients at $x = 1$ upon multiplication (i.e., $\vec{\tau}_1 \cdot \vec{f} = f(x)|_{x=1}$). Let $\vec{\tau}_2$ denote the row vector which evaluates the derivative of a Chebyshev expansion at $x = 1$ upon multiplication (i.e., $\vec{\tau}_2 \cdot \vec{f} = f'(x)|_{x=1}$). For Chebyshev polynomials,

$$(46) \quad \vec{\tau}_1 = (1, 1, 1, \dots, 1, 1), \quad \vec{\tau}_2 = (0, 1, 4, 9, \dots, i^2, \dots, M^2),$$

if $M + 1$ is the length of the expansion.

First consider Fourier modes, $n > 0$. When Poisson’s equation is solved, we choose to enforce Dirichlet boundary conditions on $\vec{\psi}_n$. The Neumann conditions on $\vec{\psi}_n$ will not be satisfied unless the right hand side ($\vec{\omega}_n$) is forced to be orthogonal to a certain

vector (solvability constraint). These solvability constraints enter the solution process when they are inserted as tau constraints in the Helmholtz operator.

One can generate these solvability constraints by replacing the last two rows of the operator (27) with Dirichlet tau conditions. Denote this $M + 1$ by $M + 1$ matrix by $\nabla_{D,n}^2$,

$$(47) \quad \nabla_{D,n}^2 \vec{\psi}_n = \mathbf{x}^2 \vec{\omega}_n,$$

where $\mathbf{x}^2 \vec{\omega}_n$ now denotes a vector whose last two components hold the boundary values $\psi_n(r)|_{r=1}$ and $\psi_n(r)|_{r=-1}$. By (22), these values are zero. Continuing,

$$\vec{\psi}_n = (\nabla_{D,n}^2)^{(-1)} (\mathbf{x}^2 \vec{\omega}_n).$$

One must require that

$$\vec{\tau}_2 \cdot \vec{\psi}_n = \vec{\tau}_2 \cdot (\nabla_{D,n}^2)^{(-1)} \mathbf{x}^2 \vec{\omega}_n = 0.$$

Defining the row vector $\vec{b}_n \equiv \vec{\tau}_2 \cdot (\nabla_{D,n}^2)^{(-1)}$ to be the solvability constraint on $\mathbf{x}^2 \vec{\omega}_n$, one has

$$(48) \quad \vec{b}_n \cdot \mathbf{x}^2 \vec{\omega}_n = 0, \quad n > 0,$$

which must be satisfied for the no-slip condition to be enforced. Take the definition of \vec{b}_n and multiply on the right by $\nabla_{D,n}^2$ to obtain

$$\vec{\tau}_2 = \vec{b}_n \cdot \nabla_{D,n}^2$$

or

$$(49) \quad (\nabla_{D,n}^2)^T \vec{b}_n^T = \vec{\tau}_2^T.$$

Thus, one can generate the solvability constraints by driving the transpose of the Dirichlet Poisson operator with a Neumann tau vector. Multiply (49) on the left by $(\mathbf{P}^2)^T$ to generate a banded system

$$(\nabla_{D,n}^2 \mathbf{P}^2)^T \vec{b}_n^T = (\vec{\tau}_2 \cdot \mathbf{P}^2)^T$$

for each Fourier mode $n > 0$. The bandwidth can again be reduced in half using the fact that \vec{b}_n will only act on vectors representing even functions for n even and vectors representing odd functions for n odd.

By (33) and (36), one has

$$\vec{\omega}_1 = R \mathbf{x} \mathbf{P}^2 \vec{s}_1^*, \quad \vec{\omega}_n = R^2 \mathbf{x}^2 \mathbf{P}^2 \vec{s}_n^*, \quad n \geq 2.$$

Since one actually solves for \vec{s}_n^* in equations (32) and (35), one must cast the solvability constraints so they act on \vec{s}_n^* . From (48) and the above equations, it is evident that

$$(50) \quad \vec{b}_1 \cdot \mathbf{x}^3 \mathbf{P}^2 \vec{s}_1^* = 0, \quad \vec{b}_n \cdot \mathbf{x}^4 \mathbf{P}^2 \vec{s}_n^* = 0, \quad n \geq 2$$

must be satisfied. Row vectors $\vec{b}_1 \cdot \mathbf{x}^3 \mathbf{P}^2$ and $\vec{b}_n \cdot \mathbf{x}^4 \mathbf{P}^2$ are inserted as tau constraints in the matrices (32) and (35). Now consider Fourier mode, $n = 0$. By (21), $\frac{d\psi_0}{dr} |_{r=R} = -U$ should be enforced.

Equation (16), $n = 0$, can be written in the form

$$(51) \quad \frac{d}{dr} \left[r \frac{d\psi_0}{dr} \right] = -r\omega_0.$$

Integrating over the disk $\int_0^{2\pi} \int_0^R$, one has

$$(52) \quad 2\pi R \frac{d\psi_0}{dr} \Big|_{r=R} = - \int_0^{2\pi} \int_0^R \omega_0 r dr d\theta = - \int_0^{2\pi} \int_0^R \omega r dr d\theta = -C = -2\pi R U.$$

Recall that C is used to denote the circulation, $C = \oint_{r=R} \vec{u} \cdot d\vec{l}$. By the first and the last term in (52), it is evident that the boundary condition (21), $n = 0$, will be enforced automatically upon solving (16) for $n = 0$.

However, since $U = u_{(r=R, t=0)}$ is a constant, the circulation $C(t) = 2\pi R U$ must also be held constant, which in turn imposes a constraint on ω_0 . The circulation is related to the zero Fourier mode of the vorticity by (25),

$$\frac{dC}{dt} = 2\pi\nu \frac{d\omega_0}{dr} \Big|_{r=R}.$$

Since C must remain constant, $\frac{dC}{dt} = 0$. Hence,

$$(53) \quad \frac{d\omega_0}{dr} \Big|_{r=R} = \frac{1}{R} \frac{d\omega_0}{dx} \Big|_{x=1} = 0.$$

Forcing the Neumann boundary condition on $\omega_0(r)$ imposes a corresponding boundary condition on \vec{s}_0^* . Enforcing $\frac{d\omega_0}{dr} \Big|_{r=R} = 0$ is equivalent to enforcing $\vec{\tau}_1 \cdot \frac{1}{R} \frac{d\vec{\omega}_0}{dx} = 0$. By (41), one has

$$(54) \quad \vec{\tau}_1 \cdot \mathbf{xP}^2 \vec{s}_0^* = 0.$$

We choose not to enforce boundary constraints by splitting the solution into a homogenous and particular part since the bounded homogenous solutions of (18) are $\omega_n = I_n(\frac{r}{\sqrt{\epsilon}})$, where I_n is the modified Bessel function of the first kind, and thus grows approximately like $\epsilon^{.25}(2\pi r)^{-.5} \exp(\frac{r}{\sqrt{\epsilon}})$ to first order, which is extremely fast for $\epsilon \ll 1$.

Additional boundary conditions at $r = 0$ in both the Poisson and Helmholtz equations arise from the differential equations themselves and the fact that the functions ψ_n and ω_n and their derivatives are assumed bounded at $r = 0$. In the code, regularity boundary conditions are not enforced since the expansion interval ranges from $[-R, R]$. Regularity boundary conditions should be satisfied automatically if the ODEs are satisfied.

4.1. Projecting initial vorticity distribution. If no-slip boundary conditions are imposed, an arbitrary vorticity distribution may not satisfy the solvability constraints, (48) and (53).

One could proceed without changing the initial vorticity. After the first iteration, the Helmholtz equation would be solved and the initial vorticity distribution would be modified to satisfy these solvability constraints. However, this approach could lead to a subsequent vorticity distribution significantly different from the intended initial distribution.

Another approach is to change the initial vorticity distribution prior to beginning the first iteration and thus exercise more control over how the initial distribution is to be modified. We choose to add sharp boundary layers to the initial distribution and thus leave the interior distribution intact.

The code takes an initial vorticity distribution $\omega(r, \theta)$, and decomposes it into its Fourier components (14). Each component of $\omega_n^c(r)$ and $\omega_n^s(r)$ is modified by adding a power of x in such a way that the solvability constraints are satisfied,

$$\omega_n(x) = \omega_n(x) + \lambda_n x^p.$$

Specifically, for $n > 0$,

$$\lambda_n = -\frac{\vec{b}_n \cdot \mathbf{x}^2 \vec{\omega}_n}{\vec{b}_n \cdot \mathbf{x}^2 \vec{x}^p}.$$

If n is even, p should be even. If n is odd, p should be odd. Typically, p is chosen to be a large number. Here \vec{x}^p is used to denote the vector of Chebyshev expansion coefficients for $\frac{r}{R}$.

For $n = 0$, λ_0 is chosen to enforce (53) and is

$$\lambda_0 = \frac{-\vec{\tau}_2 \cdot \vec{\omega}_0^c}{\vec{\tau}_2 \cdot \vec{x}^p = p}.$$

5. Conclusion. In the time integration, a Poisson equation (11) and a Helmholtz equation (12) are solved each time step.

The stream function ψ and vorticity ω are expanded in a Fourier–Chebyshev series, as shown by equations (13), (14), and (15). Due to the orthogonality of the sine and cosine functions, the 2D Poisson and Helmholtz equations can be decomposed into independent ordinary differential equations given by (16) for Poisson and (18) for Helmholtz.

For Poisson, one solves the ODEs (16) numerically by solving the system of equations (29) with the boundary conditions $\psi_n^s|_{r=R} = \psi_n^c|_{r=R} = 0$. These are enforced by requiring

$$(55) \quad \vec{\tau}_1 \cdot \vec{\psi}_n^s = \vec{\tau}_1 \cdot \vec{\psi}_n^c = 0.$$

Since the system of equations (29) operates on $(\psi_n^c)^*$ and $(\psi_n^s)^*$, the boundary constraints (55) are recast. By (28),

$$(56) \quad (\vec{\tau}_1 \cdot \mathbf{P}^2) \cdot (\psi_n^s)^* = (\vec{\tau}_1 \cdot \mathbf{P}^2) \cdot (\psi_n^c)^* = 0$$

must be enforced on $(\psi_n^c)^*$ and $(\psi_n^s)^*$.

One solves (29) with the boundary constraints (56), by replacing the last row of (29) with the boundary constraint (56). The resulting linear systems are banded with a bandwidth of 5. Using the fact that ψ_n^s and ω_n^s will have an even expansion if n is even, and an odd expansion if n is odd, one can further reduce the bandwidth of the matrix to 3 (with the exception of the tau constraint) and cut the size of the matrix in half.

For Helmholtz, one solves the ODEs (18) numerically by solving the systems of equations given by equations (32), (35), and (40) with the boundary constraints (50) and (54). The bandwidth of the matrices are reduced as with Poisson’s equation. The

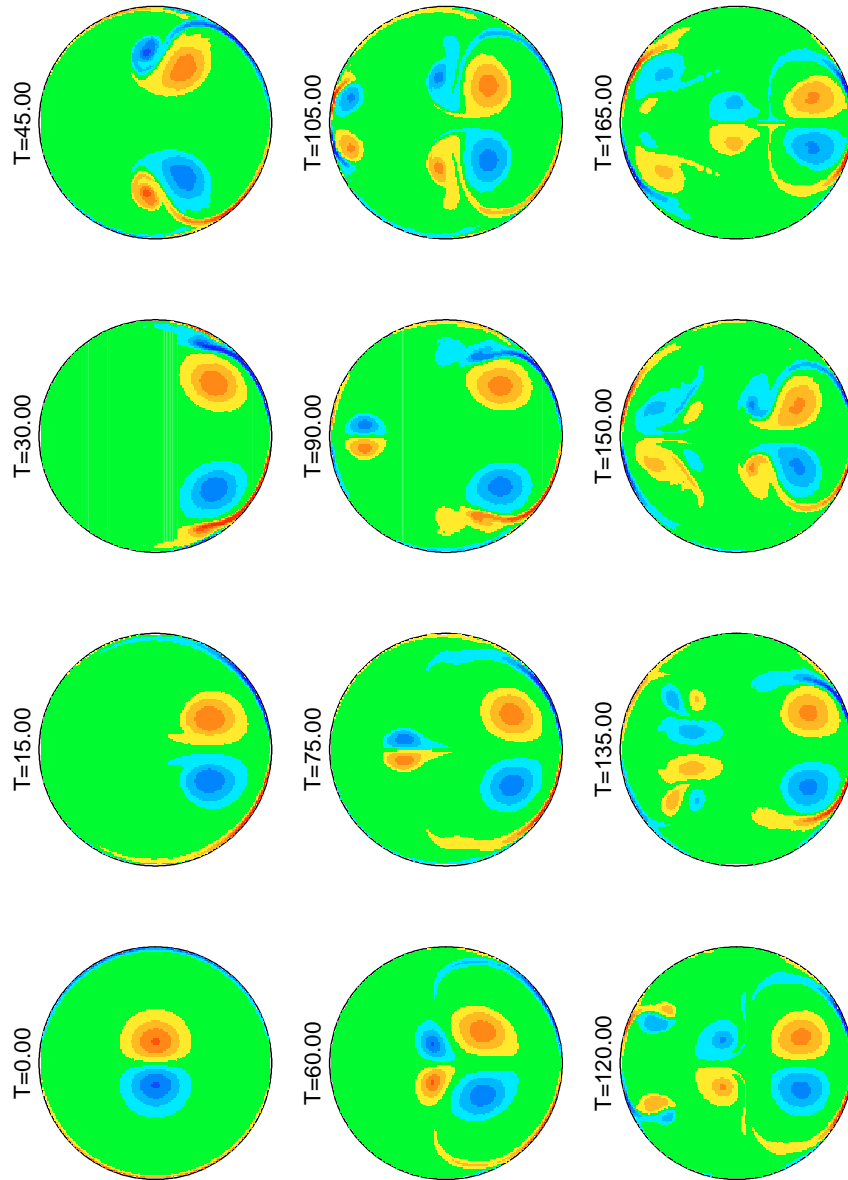


FIG. 3. Dipole collision with cylindrical wall. Eleven levels of vorticity ranging from “red” (2.0) to “blue” (−2.0) are displayed.

resulting systems have a bandwidth of 5 for (35) and 4 for (32) and (40), with the exception of the tau constraint. The vorticity is recovered using equations (33), (36), and (41), (42), and (43). These equations improve the solution of Helmholtz equation when $\epsilon \ll 1$. In computing the Jacobian, the differentiation of ψ and ω with respect to the radial coordinate can be eliminated through the use of the postconditioned method. Although the present version of the code does differentiate, the inaccuracies caused by differentiation in the Jacobian could be eliminated in a future version of

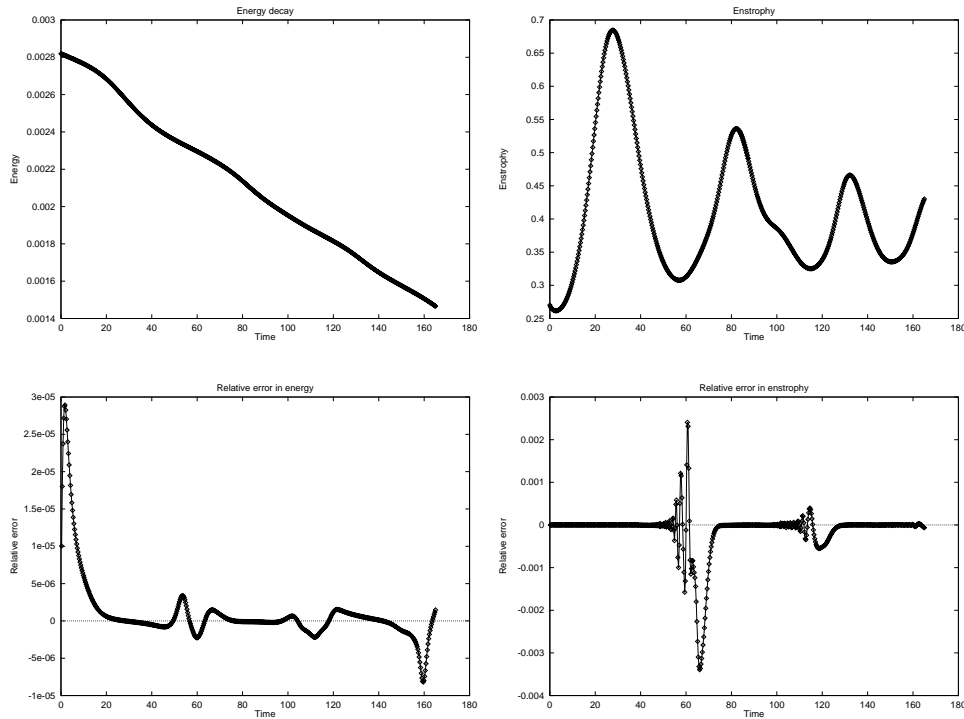


FIG. 4. *Top: Evolution of energy and enstrophy for Figure 3. Bottom: Relative errors in $\frac{dE}{dt}$ and $\frac{d\Omega}{dt}$ for Figure 3, where the exact solution was calculated using right hand sides of (23) and (24) and the approximate solution was computed by using a leapfrog scheme after calculating E and Ω at $t - \delta t$ and $t + \delta t$.*

the code.

Runs were performed in double precision. Due to the FFT-FCT and the efficient Poisson and Helmholtz solvers, $\mathcal{O}(NM \log(NM))$ operations are required to advance the solution one time step, where N is the number of Fourier modes and M is the number of Chebyshev modes.

We conclude with a simulation of a dipole colliding with a circular wall at Reynolds number (≈ 1250). The simulation was run on 4 nodes of the 32 node SP2 situated at the Albuquerque High Performance Computing Center in Albuquerque, New Mexico.

Figure 3 shows a filled-contour plot of vorticity calculated with our solution method. “Red” is positive vorticity and “blue” is negative vorticity. The radius of the disk is 1. Eleven levels of vorticity (ranging from -2.0 to 2.0) are shown. The Reynolds number $Re = \frac{R_0 U_0}{\nu}$ is calculated by setting U_0 to be the dipole velocity, and R_0 to be the distance from the center of the dipole to the location where the vorticity decays to 10 % of its maximum value. The calculation was performed with a time step of $3. \times 10^{-4}$, a viscosity of $2. \times 10^{-5}$, and a dealiased 512×512 Chebyshev–Fourier expansion under no-slip conditions. The initial maximum radial and tangential velocities are .169 and $-.169$ respectively. The initial vorticity distribution is $1.5e^{-20((x-x_1)^2+y^2)} - 1.5e^{-20((x-x_2)^2+y^2)}$, modified by the projection scheme to fit the no-slip boundary conditions, where $x_1 = .15$, $x_2 = -.15$. The average tangential velocity at the wall, $r = 1$, never exceeded 1×10^{-7} , when sampled every 1000 iterations. Thus the no-slip boundary conditions were enforced.

The dipole collides with the wall and splits, each lobe generating vorticity of the opposite sign. Each lobe pairs up with the wall vorticity it induces and two new unsymmetric vortex dipoles form which rebound from the wall in curved trajectories. These subsequently collide with each other, exchanging partners to form two symmetric almost-dipoles. The smallest moves backwards along the original path, heading for the diametrically opposed point to the first collision. The larger repeats the collision process. Three separate collision events were seen, with the secondary dipoles showing complicated interactions of their own.

The code is currently used in studies of turbulence, decaying or forced, in a circular geometry. Preliminary results were reported by Nielsen et al. [15].

Figure 4 shows the evolution of energy and enstrophy as well as relative errors in $\frac{dE}{dt}$ and $\frac{d\Omega}{dt}$. The large variations in the relative error in $\frac{d\Omega}{dt}$ suggest the use of a variable time step but also may be due to the use of a leapfrog scheme in the diagnostics. The collision events are best witnessed by the sequence of (decreasing) local maxima in the total enstrophy evolution plot.

Appendix A. Efficient solution of ODEs. Consider the ODE

$$(57) \quad Lu(x) \equiv \sum_{i=0}^n p_i(x) \frac{d^i u}{dx^i} = f(x).$$

Expanding $u(x)$ and $f(x)$ in the orthogonal polynomial family of choice

$$(58) \quad u(x) \cong \sum_{i=0}^M u_i Q_i(x), \quad f(x) \cong \sum_{i=0}^M f_i Q_i(x)$$

and employing the residual condition of the spectral τ -method yields the linear system

$$(59) \quad \mathcal{L}\vec{u} = \sum_{i=0}^n p_i(\mathbf{A}) \mathbf{D}^i \vec{u} = \vec{f}.$$

Boundary conditions are inserted by replacing the last rows of the matrix \mathcal{L} with row vectors. Let \mathcal{L} denote this matrix. \mathbf{D} is the differentiation matrix, defined by

$$(60) \quad \mathbf{D}\vec{u} = \vec{u}', \quad \text{where} \quad \frac{d}{dx} \sum_{i=0}^M u_i Q_i(x) = \sum_{i=0}^M u_i' Q_i(x),$$

and \mathbf{A} is the convolution matrix, defined by

$$(61) \quad \mathbf{A}\vec{u} = \vec{u}^x, \quad \text{where} \quad x \sum_{i=0}^M u_i Q_i(x) = \sum_{i=0}^{M+1} u_i^x Q_i(x).$$

One could potentially solve $\mathcal{L}\vec{u} = \vec{b}$. However, the number of operations is an expensive $\mathcal{O}(M^2)$ and, moreover, the matrices in this form tend to be extremely ill-conditioned. However this matrix can be banded, independent of the truncation M , allowing one to solve the system in a total of $\mathcal{O}(M)$ operations. The method relies on two recurrence relations.

It is well-known that all orthogonal polynomial families share a three-term recurrence (Abramowitz and Stegun [1]) and the three-term recurrence guarantees that \mathbf{A} is tridiagonal.

In many important cases, including the classical orthogonal polynomials (i.e., Jacobi, Chebyshev, Legendre, Gegenbauer, Hermite, and Laguerre polynomials) there also holds a relation of the form,

$$(62) \quad \sum_{l=-1}^1 Q'_{k+l} b_{k+l,k} = Q_k, \quad k = 0, 1, \dots,$$

Coutsias et al. [7]. Let $\mathbf{B} = [b_{i,j}]$ be the tridiagonal coefficient matrix in (62) and define the vectors

$$\vec{q}_x = (Q_0(x), Q_1(x), \dots, Q_M(x)),$$

$$\vec{q}'_x = (Q'_0(x), Q'_1(x), \dots, Q'_M(x)).$$

In matrix form, (62) can be written

$$(63) \quad \vec{q}'_x \cdot \mathbf{B} = (Q_0, Q_1, Q_2, \dots, Q_{M-1}, \bullet).$$

Note that an unknown term, denoted by the \bullet , is lodged in the $(M + 1)$ th column of (63). This is due to the fact that $Q_M(x)$ needs to be constructed from $Q'_{M-1}(x)$, $Q'_M(x)$, and $Q'_{M+1}(x)$. In addition, the basic recursion (62) remains unchanged regardless of how the first row of \mathbf{B} is defined since $Q'_0(x) = 0$ for polynomial families. Thus the very first row of \mathbf{B} will always be set to zero. For Chebyshev polynomials, $b_{i-1,i} = -\frac{1}{2(i-1)}$ and $b_{i+1,i} = \frac{1}{2(i+1)}$.

One can solve the set of linear equations (59) in $\mathcal{O}(M)$ operations through the use of the operator \mathbf{B} . Note that it is applicable to polynomial coefficient ODEs. This method is essentially a variation of the preconditioned approach presented in Coutsias et al. [7]. The main difference is that this implementation bands the system (59) by multiplication on the right (hence the term post-conditioned). In addition, solving the new banded system of equations is exactly equivalent to solving (59) with tau constraints, neglecting round-off error.

A.1. Building the postconditioner for \mathbf{D} . Assume $f(x)$ is a sum of orthogonal polynomials ($f(x) = \vec{q}_x \cdot \vec{f}$) whose degrees range from 0 to M . Recall the two ways in which $f'(x)$ can be represented

$$(64) \quad f'(x) = \vec{q}'_x \cdot \vec{f} = \vec{q}_x \cdot \vec{f}',$$

defining f' to be $\mathbf{D}\vec{f} = \vec{f}'$. Note that the last element of \vec{f}' is zero since the highest degree present in the function $f'(x)$ is $M - 1$.

Since the last entry of the vector \vec{f}' is zero, one has (by multiplying (63) on the right by \vec{f}')

$$(65) \quad \vec{q}'_x \cdot \mathbf{B}\vec{f}' = \vec{q}_x \cdot \vec{f}'.$$

Combining (64) with (65), one obtains

$$(66) \quad \vec{q}'_x \cdot \mathbf{B}\vec{f}' = \vec{q}'_x \cdot \vec{f}$$

or

$$(67) \quad \vec{q}'_x \cdot (\mathbf{B}\vec{f}' - \vec{f}) = 0.$$

Now \vec{q}_x is composed of orthogonal and therefore independent functions Q'_i (with the exception of $Q'_0 = 0$). As a result, one has from (67)

$$(68) \quad \mathbf{B}\vec{f}' = \vec{f}' + \vec{c},$$

where \vec{c} is a column vector of the form $\vec{c}^T = (\bullet, 0, 0, 0, \dots, 0)$. The superscript T denotes the transpose. Hence \mathbf{B} acts as an “integration operator”.

The first column of all differentiation matrices is full of zeroes (since Q_0 becomes 0 upon differentiation). By multiplying (68) by \mathbf{D} , one obtains

$$(69) \quad \mathbf{D}\vec{f}' = \mathbf{D}\mathbf{B}\vec{f}'.$$

Upon substituting \vec{f}' for $\mathbf{D}\vec{f}'$, (69) assumes the form

$$(70) \quad \vec{f}' = \mathbf{D}\mathbf{B}\vec{f}'.$$

Since \vec{f}' is any arbitrary vector, except for a zero in its last entry, (70) implies that

$$(71) \quad (\mathbf{D}\mathbf{B})_{(1)} = \mathbf{I}_{(1)}$$

where \mathbf{I} denotes the identity matrix and $\mathbf{G}_{<k>}$ denotes any matrix with its last k columns set to zero.

Define the following $M + 1$ by $M + 1$ matrices \mathbf{S}_1 and \mathbf{S}_{1-} . \mathbf{S}_1 is the $M + 1$ Jordan block (i.e., a matrix whose superdiagonal is filled with ones),

$$(72) \quad (\mathbf{S}_1)_{ij} \equiv \begin{cases} 1, & j = i + 1, \\ 0 & \text{otherwise,} \end{cases}$$

while \mathbf{S}_{1-} is a matrix whose subdiagonal is filled with ones, $\mathbf{S}_{1-} = \mathbf{S}_1^T$.

From (71) and the definition of \mathbf{S}_1 , one can verify that

$$(73) \quad \mathbf{D}\mathbf{B}\mathbf{S}_1 = \mathbf{S}_1.$$

Recall that the first column of \mathbf{D} is full of zeroes. Thus, the equation (73) will not be affected if the first row of $\mathbf{B}\mathbf{S}_1$ is modified. Substitute 1 in the (1,1) location of $\mathbf{B}\mathbf{S}_1$ and zero out any other nonzero entries present in the first row. Call this new matrix \mathbf{B}^*_{1} . Thus, one can state

$$(74) \quad \mathbf{D}\mathbf{B}^*_{1} = \mathbf{S}_1,$$

where the $M + 1$ by $M + 1$ matrix

$$\mathbf{B}^*_{1} = \begin{bmatrix} 1 & 0 & 0 & 0 & 0 & 0 \\ 0 & b_{1,0} & b_{1,1} & b_{1,2} & 0 & 0 \\ 0 & 0 & b_{2,1} & b_{2,2} & b_{2,3} & 0 \\ 0 & 0 & 0 & b_{3,2} & b_{3,3} & \ddots \\ 0 & 0 & 0 & 0 & \ddots & \ddots \end{bmatrix}.$$

Note that \mathbf{B}^*_{1} will be nonsingular as the $b_{k,k-1}$'s are nonzero for the Jacobi, Hermite, and Laguerre polynomials by Coutsiyas et al. [7]. Thus one now has a nonsingular matrix (\mathbf{B}^*_{1}) that transforms the upper triangular matrix \mathbf{D} into the simple matrix \mathbf{S}_1 .

A.2. Building the postconditioner for D^2 . Now, this process is extended to higher powers of D . Start with D^2 . One can show that $S_1^k S_{1-}^k = I_{(k)}$.

Multiplying $DB^*_1 = S_1$ by S_{1-} and using the equation $S_1 S_{1-} = I_{(1)}$, one obtains

$$(75) \quad DB^*_1 S_{1-} = I_{(1)}.$$

Multiplying (75) on the left by D , one obtains

$$(76) \quad D^2 B^*_1 S_{1-} = D_{(1)}.$$

Multiplying (76) on the right by B^*_1 yields (via equation (74) and the fact that B^*_1 is upper triangular)

$$(77) \quad (D^2 B^*_1 S_{1-} B^*_1)_{(1)} = (S_1)_{(1)}.$$

Multiplying (77) by S_1 leads to

$$(78) \quad D^2 B^*_1 (S_{1-} B^*_1 S_1) = S_1^2.$$

Note that D^2 will have its first two columns full of zeros. Since B^*_1 is upper triangular, $D^2 B^*_1$ will also have its first two columns full of zeros. Thus (78) will not be affected if the first two rows of $S_{1-} B^*_1 S_1$ are modified. Only the (1,1) element of $S_{1-} B^*_1 S_1$ will actually be changed from 0 to 1. Call the new $M + 1$ by $M + 1$ matrix B^*_2 ,

$$B^*_2 \equiv \begin{bmatrix} 1 & 0 & 0 & 0 & 0 & 0 & 0 \\ 0 & 1 & 0 & 0 & 0 & 0 & 0 \\ 0 & 0 & b_{1,0} & b_{1,1} & b_{1,2} & 0 & 0 \\ 0 & 0 & 0 & b_{2,1} & b_{2,2} & \ddots & 0 \\ 0 & 0 & 0 & 0 & \ddots & \ddots & \ddots \end{bmatrix},$$

which is also a nonsingular upper triangular matrix. Thus

$$(79) \quad D^2 B^*_1 B^*_2 = S_1^2.$$

A.3. Building the postconditioner for D^i . The process can now propagate itself through induction to higher powers of D . First define B^*_{j+1} to be the matrix $(S_{1-}^j B^*_1 S_1^j)$ with its (1, 1), (2, 2), (3, 3), ..., (j, j) elements replaced by 1. Zeroes previously occupied these positions. More simply, B^*_{j+1} is B^*_1 shifted j units diagonally downward, leaving the first j columns and rows vacant. B^*_{j+1} fills the first j vacant diagonal entries with ones. In general,

$$(80) \quad D^i \left(\prod_{j=1}^i B^*_j \right) = S_1^i.$$

Right multiplication by $S_{1-}^i B^*_1 S_1^i$ and left multiplication by D yields

$$(81) \quad D^{i+1} \left(\prod_{j=1}^i B^*_j \right) S_{1-}^i B^*_1 S_1^i = S_1^{i+1}.$$

Now \mathbf{D}^{i+1} has $i + 1$ zero first columns. In addition \mathbf{B}^*_j , $j \leq i$ are all upper triangular matrices. Thus $\mathbf{D}^{i+1}(\prod_{j=1}^i \mathbf{B}^*_j)$ will be a matrix with $i + 1$ zero first columns. Therefore, (81) will not be affected if $(\mathbf{S}_1^i - \mathbf{B}^* \mathbf{S}_1^i)$ is replaced by \mathbf{B}^*_{i+1} . Equation (81) can now be restated in the form

$$(82) \quad \mathbf{D}^{i+1} \left(\prod_{j=1}^{i+1} \mathbf{B}^*_j \right) = \mathbf{S}_1^{i+1},$$

where

$$(83) \quad \mathbf{B}^*_j \equiv \begin{bmatrix} 1 & 0 & 0 & 0 & 0 & 0 & \cdots & 0 \\ 0 & \ddots & 0 & 0 & 0 & 0 & \cdots & 0 \\ 0 & 0 & 1 & 0 & 0 & 0 & \cdots & 0 \\ 0 & 0 & 0 & b_{1,0} & b_{1,1} & b_{1,2} & 0 & \cdots \\ 0 & 0 & 0 & 0 & b_{2,1} & b_{2,2} & b_{2,3} & \cdots \\ 0 & 0 & 0 & 0 & 0 & \ddots & \ddots & \ddots \end{bmatrix}.$$

The row vector $(0, 0, 0, b_{1,0}, b_{1,1}, b_{1,2}, 0, \dots)$ is the $(j + 1)$ th row of \mathbf{B}^*_j . Thus, by induction, a nonsingular banded matrix (which we will denote \mathbf{P}^i)

$$\mathbf{P}^i \equiv \prod_{j=1}^i \mathbf{B}^*_j$$

has been constructed, which transforms \mathbf{D}^i into \mathbf{S}_1^i for any i upon right multiplication. The entries $b_{i,j}$ are determined by the recurrence relation (62), the values of which are given in [7] for many classical orthogonal polynomials. \mathbf{P}^i is upper triangular with a bandwidth of $2i + 1$.

A.4. \mathbf{P}^i bands lower powers of \mathbf{D} . Note that \mathbf{P}^i also bands \mathbf{D}^j for $j < i$, since

$$(84) \quad \mathbf{D}^j \mathbf{P}^i = \mathbf{D}^j \prod_{k=1}^i \mathbf{B}^*_k = \left(\mathbf{D}^j \prod_{k=1}^j \mathbf{B}^*_k \right) \left(\prod_{k=j+1}^i \mathbf{B}^*_k \right) = \mathbf{S}_1^j \left(\prod_{k=j+1}^i \mathbf{B}^*_k \right).$$

All matrices in the right hand side of the last equality are banded. Thus $\mathbf{D}^j \mathbf{P}^i$ is a banded matrix.

A.5. Summary. Equation (59) represents the standard matrix that arises (with tau constraints in the last $n -$ rows) when the ODE (57) is solved using a spectral expansion. Begin by making the substitution

$$(85) \quad \vec{u} = \mathbf{P}^n \vec{z},$$

where \mathbf{P}^n is the nonsingular matrix (from the previous subsection) that reduces \mathbf{D}^n to the simple matrix \mathbf{S}_1^n upon right multiplication. \mathbf{P}^n also bands all lower order powers of \mathbf{D}^i , $i < n$ by (84). Equation (59) now assumes the form

$$\mathcal{L} \mathbf{P}^n \vec{z} = \vec{b}.$$

Now $\mathcal{L} \mathbf{P}^n$ is a banded matrix (except for the tau conditions) for the following reasons:

(i) The 1 row to the $M + 1 - n$ row are essentially the first through $M + 1 - n$ rows of the matrix $(\sum_{i=0}^{i=n} p_i(\mathbf{A})\mathbf{D}^i)\mathbf{P}^n$. The tau constraints are mapped into new row vectors in the last n rows.

(ii) The matrices $\mathbf{D}^i\mathbf{P}^n$ are all banded matrices.

(iii) The matrices $p_i(\mathbf{A})$ are banded matrices since \mathbf{A} is a banded matrix. After \vec{z} has been solved, \vec{u} is recovered via the banded multiplication $\vec{u} = \mathbf{P}^n\vec{z}$, which is another $\mathcal{O}(M)$ operation.

Appendix B. Conditioning. This appendix supplies the details in deriving the condition numbers in section 3.4. Begin with equations (44) and (45). Consider the perturbed system,

$$(86) \quad (\mathbf{A} + \Delta\mathbf{A})(\vec{s}^* + \Delta\vec{s}^*) = \vec{f} + \Delta\vec{f}$$

and

$$(87) \quad \vec{u} + \Delta\vec{u} = (\mathbf{x}^l + \Delta\mathbf{x}^l)(\mathbf{P}^2 + \Delta\mathbf{P}^2)(\vec{s}^* + \Delta\vec{s}^*).$$

Using (44) and (86), and assuming $\|\mathbf{A}^{-1}\| \|\Delta\mathbf{A}\| < 1$, one can show

$$(88) \quad \Delta\vec{s}^* = \mathbf{A}^{-1}\Delta\vec{f} + \sum_{k=1}^{\infty} (-1)^k (\mathbf{A}^{-1} \Delta\mathbf{A})^k \mathbf{A}^{-1}(\vec{f} + \Delta\vec{f}).$$

Subtracting (45) from (87), and combining the result with (88), yields

$$(89) \quad \begin{aligned} \Delta\vec{u} &= (\mathbf{x}^l \Delta\mathbf{P}^2 + \Delta\mathbf{x}^l \mathbf{P}^2 + \Delta\mathbf{x}^l \Delta\mathbf{P}^2) \vec{s}^* \\ &+ (\mathbf{x}^l \mathbf{P}^2 + \mathbf{x}^l \Delta\mathbf{P}^2 + \Delta\mathbf{x}^l \mathbf{P}^2 + \Delta\mathbf{x}^l \Delta\mathbf{P}^2) \mathbf{A}^{-1} \Delta\vec{f} \\ &+ (\mathbf{x}^l \mathbf{P}^2 + \mathbf{x}^l \Delta\mathbf{P}^2 + \Delta\mathbf{x}^l \mathbf{P}^2 + \Delta\mathbf{x}^l \Delta\mathbf{P}^2) \sum_{k=1}^{\infty} (-1)^k (\mathbf{A}^{-1} \Delta\mathbf{A})^k \mathbf{A}^{-1}(\vec{f} + \Delta\vec{f}). \end{aligned}$$

Let Λ denote the third term in the sum on the right hand side. Using (44), one can write

$$\begin{aligned} \Lambda &= \mathbf{x}^l \mathbf{P}^2 \mathbf{A}^{-1} \left(\sum_{k=1}^{\infty} (-1)^k (\Delta\mathbf{A} \mathbf{A}^{-1})^{k-1} \right) \Delta\mathbf{A} (\vec{s}^* + \mathbf{A}^{-1} \Delta\vec{f}) \\ &+ (\mathbf{x}^l \Delta\mathbf{P}^2 + \Delta\mathbf{x}^l \mathbf{P}^2 + \Delta\mathbf{x}^l \Delta\mathbf{P}^2) \left(\sum_{k=1}^{\infty} (-1)^k (\mathbf{A}^{-1} \Delta\mathbf{A})^k \right) (\vec{s}^* + \mathbf{A}^{-1} \Delta\vec{f}). \end{aligned}$$

Taking norms one has

$$\begin{aligned} \|\Lambda\| &\leq \|\Delta\mathbf{A}\| \left(\|\vec{s}^*\| + \|\mathbf{A}^{-1}\| \|\Delta\vec{f}\| \right) * \\ &\left(\|\mathbf{x}^l \mathbf{P}^2 \mathbf{A}^{-1}\| + \|\mathbf{A}^{-1}\| \left[\|\mathbf{x}^l\| \|\Delta\mathbf{P}^2\| + \|\Delta\mathbf{x}^l\| \|\mathbf{P}^2\| + \|\Delta\mathbf{x}^l\| \|\Delta\mathbf{P}^2\| \right] \right) B, \end{aligned}$$

where

$$B = \frac{1}{1 - \|\Delta\mathbf{A}\| \|\mathbf{A}^{-1}\|}.$$

Taking the norm of (89), dividing by $\|\vec{s}^*\|$, and using the norm inequality from (44),

$$\frac{1}{\|\vec{s}^*\|} \leq \frac{\|A\|}{\|f\|},$$

one can show after some algebra,

$$\begin{aligned} \frac{\|\vec{\Delta}u\|}{\|\vec{s}^*\|} &\leq \|\mathbf{x}^l\| \|\mathbf{P}^2\| \left(\delta P + \delta x + \delta x \delta P \right) \\ &+ \left(\|\mathbf{x}^l \mathbf{P}^2 \mathbf{A}^{-1}\| \|\mathbf{A}\| + C_A \|\mathbf{x}^l\| \|\mathbf{P}^2\| (\delta x + \delta P + \delta x \delta P) \right) \left(\delta f + B[1 + C_A \delta f] \delta A \right), \end{aligned}$$

where

$$\delta A = \frac{\|\Delta \mathbf{A}\|}{\|\mathbf{A}\|}, \quad \delta P = \frac{\|\Delta \mathbf{P}^2\|}{\|\mathbf{P}^2\|}, \quad \delta x = \frac{\|\Delta \mathbf{x}^l\|}{\|\mathbf{x}^l\|}, \quad \delta f = \frac{\|\vec{\Delta}f\|}{\|\vec{f}\|},$$

and $C_A = \|\mathbf{A}\| \|\mathbf{A}^{-1}\|$. Now assume

$$(90) \quad \frac{\|\vec{u} = \mathbf{x}^l \mathbf{P}^2 \vec{s}^*\|}{\|\vec{s}^*\|} \geq \alpha,$$

where α is a positive constant. Using (90) generates

$$(91) \quad \frac{\|\vec{\Delta}u\|}{\|\vec{u}\|} \leq \frac{1}{\alpha} \|\mathbf{x}^l\| \|\mathbf{P}^2\| \delta(xP) + \frac{1}{\alpha} \left(\|\mathbf{x}^l \mathbf{P}^2 \mathbf{A}^{-1}\| \|\mathbf{A}\| + C_A \|\mathbf{x}^l\| \|\mathbf{P}^2\| \delta(xP) \right) \left(\delta f + B[1 + C_A \delta f] \delta A \right)$$

where

$$\delta(xP) = (\delta x + \delta P + \delta x \delta P).$$

Neglecting higher order errors and δx and δP , the effective condition number is

$$\frac{\|\vec{\Delta}u\|}{\|\vec{u}\|} \leq \frac{1}{\alpha} \|\mathbf{x}^l \mathbf{P}^2 \mathbf{A}^{-1}\| \|\mathbf{A}\| \left(\delta f + 2\delta A \right).$$

Acknowledgements. We would like to acknowledge the use of the SP2 computer at the Albuquerque High Performance Computing Center. The authors would like to acknowledge helpful conversations with J. P. Lynov, J. P. Boyd, B. Fornberg, and T. Hagstrom.

REFERENCES

- [1] M. ABRAMOWITZ AND I.A. STEGUN, *Handbook of Mathematical Functions*, Dover, New York, 1965.
- [2] U. ASCHER, S. RUUTH, AND B. WETTON, *Implicit-explicit methods for time-dependent partial differential equations*, SIAM J. Numer. Anal., 32 (1995), pp. 797–823.
- [3] J. P. BOYD, *Chebyshev & Fourier Spectral Methods*, Springer-Verlag, Berlin, Heidelberg, 1989.
- [4] C. CANUTO, M. Y. HUSSAINI, A. QUARTERONI, AND T. A. ZANG, *Spectral Methods in Fluid Dynamics*, Springer-Verlag, New York, 1988.

- [5] E. A. COUTSIAS AND J. P. LYNNOV, *Fundamental interactions of vortical structures with boundary layers in two-dimensional flows*, *Physica D*, 51 (1991), pp. 482–497.
- [6] E. A. COUTSIAS, T. HAGSTROM, AND D. TORRES, *An efficient spectral method for ordinary differential equations with rational function coefficients*, *Math. Comp.*, 65 (1996), pp. 611–635.
- [7] E. A. COUTSIAS, T. HAGSTROM, J. S. HESTHAVEN, AND D. TORRES, *Integration preconditioners for differential operators in spectral τ -methods*, in proceedings of the International Conference on Spectral and Higher Order Methods, R. Scott, ed., Houston, 1995; to appear in a special issue of *Houston J. Math.*
- [8] S. C. R. DENNIS AND L. QUARTAPELLE, *Direct solution of the vorticity-stream function ordinary differential equations by a Chebyshev approximation*, *J. Comput. Phys.*, 52 (1983), p. 448.
- [9] H. EISEN, W. HEINRICHS, AND K. WITSCH, *Spectral collocation methods and polar coordinate singularities*, *J. Comput. Phys.*, 96 (1991), pp. 241–257.
- [10] B. FORNBERG, *A pseudospectral approach for polar and spherical geometries*, *SIAM J. Sci. Comput.*, 16 (1995), pp. 1071–1081.
- [11] D. GOTTLIEB AND S. ORSZAG, *Numerical Analysis of Spectral Methods*, SIAM, Philadelphia, PA, 1977.
- [12] W. HUANG AND D. SLOAN, *Pole condition for singular problems: The pseudospectral approximation*, *J. Comput. Phys.*, 107 (1993), pp. 254–261.
- [13] T. MATSUSHIMA AND P. S. MARCUS, *A spectral method for polar coordinates*, *J. Comput. Phys.*, 120 (1995), pp. 365–374.
- [14] P. E. MERILEES, *An alternative scheme for the summation of a series of spherical harmonics*, *J. Appl. Meteor.*, 12 (1973), pp. 224–227.
- [15] A. H. NIELSEN, D. TORRES, AND E. A. COUTSIAS, *Decaying two-dimensional turbulence in bounded flows*, in Proceedings of the International Congress on Plasma Physics and the 25th EPS Conference on Controlled Fusion and Plasma Physics, 1998.
- [16] S. A. ORSZAG, A. T. PATERA, AND R. BALASUBRAMANIAN, *Spectral Methods for Flows in Complex Geometries*, Paper 83-0229, American Institute of Aeronautics and Astronautics, Washington, D.C.
- [17] V. G. PRIYMAK, *Pseudospectral algorithms for Navier–Stokes simulation of turbulent flows in cylindrical geometry with coordinate singularities*, *J. Comput. Phys.*, 118 (1995), pp. 366–379.
- [18] V. G. PRIYMAK AND T. MIYAZAKI, *Accurate Navier–Stokes investigation of transitional and turbulent flows in a circular pipe*, *J. Comput. Phys.*, 141 (1998), pp. 1–42.
- [19] J. SHEN, *Efficient spectral-Galerkin methods III. Polar and cylindrical geometries*, *SIAM J. Sci. Comput.*, 18 (1997), 1583–1604 .
- [20] C. TEMPERTON, *Self-sorting mixed-radix fast Fourier transforms*, *J. Comput. Phys.*, 52 (1983), pp. 1–23.
- [21] D. TORRES, *Integration Operators in the Spectral τ -Method with Navier–Stokes Applications*, Ph.D. thesis, University of New Mexico, Albuquerque, NM, 1995.
- [22] W. T. VERKLEY, *A Pseudo-spectral model for two-dimensional incompressible flow in a circular basin, I. Mathematical formulation*, *J. Comput. Phys.*, 136 (1997), pp. 100–114.
- [23] W. T. VERKLEY, *A pseudo-spectral model for two-dimensional incompressible flow in a circular basin, II. Numerical examples*, *J. Comput. Phys.*, 136 (1997), pp. 115–191.